#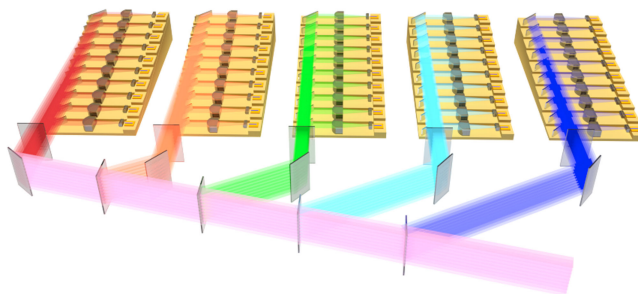 Development and Thermal Management of kW-Class High-Power Diode Laser Source Based on the Structure of Two-Stage Combination

Hongbo Zhu
Shengli Fan
Jian Zhao
Xingchen Lin
Li Qin
Yongqiang Ning

Development and Thermal Management of kW-Class High-Power Diode Laser Source Based on the Structure of Two-Stage Combination

Hongbo Zhu,[1,2] **Shengli Fan,**[2] **Jian Zhao,**[2] **Xingchen Lin,**[1] **Li Qin,**[1]
and Yongqiang Ning[1]

[1]State Key Laboratory of Luminescence and Applications, Changchun Institute of Optics, Fine Mechanics and Physics, Chinese Academy of Sciences, Changchun 130033, China
[2]CREOL, College of Optics and Photonics, University of Central Florida, Orlando, FL 32816, USA

Abstract: In this paper, we present an optical structure for two-stage beam combination to realize a high-power fiber-coupled diode laser source. In the first stage, dense spectral combination based on reflecting volume Bragg gratings is implemented for combining five diode laser blocks with a spectral separation of 1.5 nm, to a high output power submodule. In the second stage, submodules are further coaxially multiplexed by polarization beam combination and coarse spectral combination to obtain a higher output power. In the process of the beam combination, thermal effects of combining elements are also investigated. By using a temperature control, the diode laser source can steadily produce 3120-W power from an optical fiber with 105-μm core diameter and 0.2 numerical aperture. This paper demonstrates the benefits of this combination structure and the effectiveness of the temperature control.

Index Terms: Diode laser, high power, laser beam multiplexing, thermal control, volume Bragg gratings.

1. Introduction

Due to the advantages of excellent electro-optical (E-O) conversion efficiency and high output power, direct diode laser sources are desired in many industrial applications, either direct processing applications [1], or pumping other types of lasers [2], [3]. However, because of brightness limitations, diode laser sources are still not capable to be applied in many aspects of applications, such as fine processing. Over the last decade, many research groups and companies have contributed much effort to develop many novel technologies in overcoming this limitation [4], [5]. An effective way to scale the output power and modify the brightness is wavelength beam combination (WBC), where output beams from many emitters in the diode laser bars are directed to the surface diffraction grating for operating as one emitter. TeraDiode reported 4 kW output power from an optical fiber with 100 μm core diameter and 0.08 numerical aperture (NA) [6]. Additionally, dense spectral combination (DSC) based on the volume Bragg gratings (VBGs), as an alternative method of WBC, has been investigated because it can combine the arbitrary number of beamlets. In DSC,

a VBG, recorded in photo thermo-refractive (PTR) glass, serves as the optical combining element for diffracting a resonant wavelength beamlet and transmitting another non-resonant wavelength beamlet, then coaxially combining two beamlets at the VBG output. In the low power range of beam combination, experiments of DSC with spectral separations up to 1.7 nm have been reported, owing to the small wavelength shift of diode lasers and the low thermal effect of VBGs [7]. However, in the kW range of the beam combination, the wavelength shift of diode lasers and the laser-induced temperature elevating of VBGs pose many challenges, which can cause a mismatch between the spectrum of diode lasers and Bragg wavelength of VBGs. It is therefore necessary to keep a wide bandwidth of spectral selectivity of VBGs in the design to maintain the condition of Bragg resonance. To the best of our knowledge, existing VBG-based DSC technologies demand a spectral separation of ≥ 4 nm between wavelength channels [8]. Nevertheless, the diffraction bandwidth of VBGs and the gain bandwidth of diode chips limit the available spectral width in DSC, so a narrower spectral separation can make more combining channels and higher brightness possible.

In this paper, a two-stage beam combination structure with DSC and coarse spectral combination (CSC) is introduced. By investigating thermal effects and implementing a temperature control for combining elements, we realize DSC of diode laser blocks with a spectral separation of 1.5 nm. The thermal stress on the dielectric mirrors is also reduced; as a result, a direct diode laser source can steadily produce 3120 W power from an output fiber with 105 μm core diameter and 0.2 NA.

2. Optimizing of External Cavity Parameters

In DSC based on reflecting VBGs, a stable and narrow spectrum is crucial. An easy way to satisfy this requirement is to place a VBG for spectral locking in front of a diode laser emitter. The beam emitted from the emitter is reflected back into its cavity by the VBG, and its electrical field interferes with the internal electrical field of the cavity, which can influence the distribution of charged carriers and further change the refractive index inside the cavity, therefore spectral characteristics are modified [9], [10]. At this time, the output power of the emitter and the characteristics of the locked spectrum are determined by the reflectance of VBG and emitter facet. Assuming the material gain of diode chips varies linearly with the distribution of carriers, a calculation formula for the efficient spectrum locking is obtained by using rate equation analysis [11]

$$R_{\text{VBG}} \geq R_f \exp \left\{ 2\Gamma \lfloor g\left(\lambda_0\right)\rfloor - g\left(\lambda_g\right) L \right\}, \tag{1}$$

where R_f and R_{VBG} are the reflectance of the front facet and VBG, respectively. Γ is the confinement index of the gain medium, $g\left(\lambda_0\right)$ and $g\left(\lambda_g\right)$ are the medium gain at the free-running wavelength and locking wavelength of VBG, and L is the length of the emitter cavity. Eq. (1) indicates that the combination of high VBG feedback and low front facet reflectance is beneficial to spectrum locking. We take the emitter with a wavelength of 976 nm as an example. To quantize these two parameters, an analysis model for transverse and longitudinal mode selection is built using Crosslight software. The effect of transverse electrical, thermal, and optical fields with attached external feedback is implemented in this three dimensional model [12]. The optical parameters of the analysis model are set according to the actual parameters of the external cavity. Bragg condition is related to the narrow divergence angle of the beam, so the emitted beam is respectively collimated by the fast axis collimator (FAC) and slow axis collimator (SAC) which are coated with a reflectance below 0.01%. The effective focal lengths of FAC and SAC are 0.9 mm and 14 mm, respectively. A schematic diagram is shown in Fig. 1.

We examine five different front facet reflectances, ranging from $R_f < 0.05\%$ to 5%, in the combination with three different VBG reflectances of $R_{\text{VBG}} = 10\%$, 15% and 20%, respectively. A detailed numerical calculation of the output power has been performed, which is shown in Fig. 2.

From Fig. 2, we can see that all curves have a similar tendency, i.e., for a given front facet reflectance, the overall output power decreases with the increasing R_{VBG}. When the emitter is prepared with $R_f < 1\%$, the increasing R_f contributes to reduce threshold current, which can increase the output power. However, the output power drops almost linearly when $R_f > 1\%$, as more light is reflected into the cavity. At the point of $R_f = 0.5\%$ and under the condition of R_{VBG}
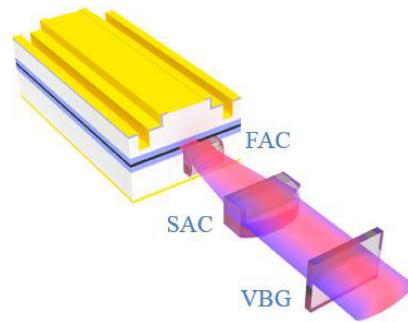
Fig. 1. Schematic diagram of external cavity system with FAC (fast axis collimator), SAC (slow axis collimator) and VBG (volume Bragg grating).
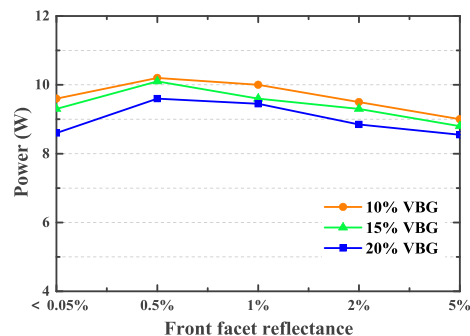

Fig. 2. Output power of the emitter with different front facet reflectances. The pump current is 10 A, and the temperature of water coolant is set to be 298 K.

$= 15\%$ and 20%, respectively, the emitter is fully wavelength locked from the threshold current to 10 A, with no side peaks and the spectral full width at half maximum (FWHM) $\Delta\lambda < 0.3$ nm. Lower R_{VBG} values (e.g., $R_{VBG} = 10\%$) are anticipated to produce higher output power, but the eigen spectrum in the internal cavity is not completely suppressed, which results in the decrease of combining efficiency. Although low power loss is desired for high efficient beam combination, to be usable in DSC, the emitter should operate at a narrow and stable spectrum. However, $R_{VBG} = 20\%$ for high locking performance can bring high risk for the reliability of the emitter [13]. Therefore, a trade-off between the output power and spectral parameters is made for designing the external cavity system. The R_{VBG} and R_f are set to be 15% and 0.5%, respectively.

The measured laser spectra before and after the wavelength locking are shown in Fig. 3. When the emitter is wavelength locked, the spectrum is narrowed from 4.2 nm to 0.3 nm, which significantly benefits from the suppression of longitudinal multi-mode of emitter. Meanwhile, the shift of the central wavelength decreases from 1.5 nm/A to 0.03 nm/A. From Eq. (1) we also know that the wavelength locking only works when λ_0 is close to λ_g. In our case, we select desired diode laser chips whose free-running wavelengths are close to Bragg wavelengths of VBGs. Some other methods, for instance, adjusting the temperature of the water cooling for diode lasers, have been reported to reduce the mismatch between the diode laser spectrum and Bragg wavelength [14]. However, it may lead to an unsatisfactory heat dissipation and the degradation of diode lasers.

3. Design of Beam Combination

3.1 Optical Stacking

In many methods for increasing output power of diode laser source, the optical stacking of multiple single diode laser emitters has been demonstrated to an efficient method, at present, because of its simple installation and adjustment [15], [16]. To do so, single emitters with an emitting width of
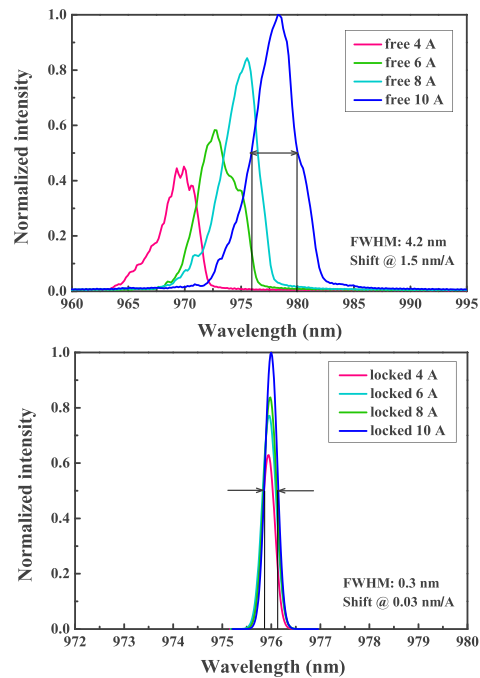
Fig. 3. The measured laser spectra as functions of pump current for 976 nm single emitter without (top) and with wavelength locking (bottom).

95 μm are employed. Each single emitter can maximally produce a CW power of 10 W at a pump current of 10 A (2% front facet reflectance), corresponding to an E-O efficiency of 55%. According to the previous analysis, emitters are coated with a front facet reflectance of 0.5%. Ten identical emitters are soldered on a cooper heatsink with a staircase shape by a process of reflow soldering. The divergent beam emitted from each single emitter is collimated using a FAC and a SAC. After collimation, the beam parameter product (BPP) is 0.37 mm·mrad in FA and 3.7 mm·mrad in SA, which is calculated by Eq. (2),

$$BPP = d_0/2 \cdot \theta_0, \tag{2}$$

where d_0 and θ_0 are the beam diameter and the half divergence angle, respectively. In order to make a balanced beam quality between FA and SA, ten reflectors are aligned to stack collimated beams in the FA direction. When a wavelength-customized VBG for spectrum locking is subsequently inserted in the output beam, we can obtain a diode laser block with a narrow and locked spectrum.

3.2 Dense Spectral Combination

In DSC, the spectral separation between wavelength channels is usually reduced for increasing the number of combining channels within an available spectrum range. Therefore, a DSC model based on five wavelength channels with a spectral separation of 1.5 nm is introduced. Firstly, we take the submodule of 97× nm wavelength as an example. According to the method described above, five diode laser blocks whose wavelengths are locked at 973.0, 974.5, 976.0, 977.5 and 979.0 nm are prepared. Characteristics of output power, center wavelength and spectral width (FWHM) of each channel are shown in Fig. 4.

A cascade structure based on the reflecting VBGs is used to combine five blocks, so four identical VBGs are used in this structure. Since the incident angels of VBGs are different for each wavelength channel, VBGs should be accurately adjusted for matching Bragg resonance condition of each channel. The schematic diagram of the 97× nm submodule is shown in Fig. 5. Incident
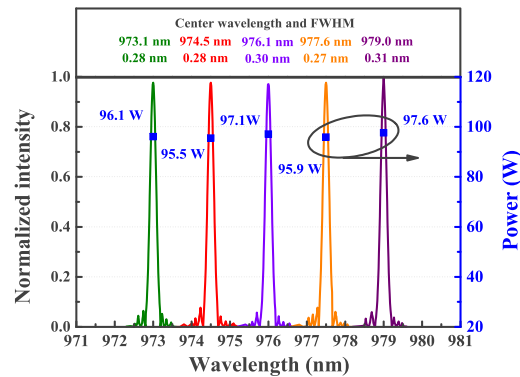
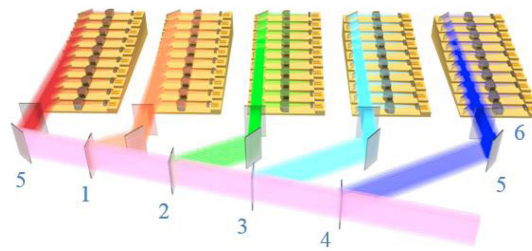Fig. 4. Spectral characteristics of five channels in the 97× nm diode laser submodule.

Fig. 5. Schematic diagram of 97× nm diode laser submodule based on the DSC. 1-4: VBG for combination, 5: reflector, 6: VBG for wavelength locking.

angles are determined from the Bragg diffraction equation

$$|\cos\theta_0| = \frac{\lambda}{2\Lambda n_{av}}, \tag{3}$$

where θ_0 is incident angle of VBG, λ is the wavelength of each channel, Λ is the VBG period, and n_{av} is the average refractive index of VBG [17]. From the above equation, incident angles of five channels are calculated to be 16.536°, 15.737°, 14.949°, 14.225° and 13.410°, respectively.

From Fig. 5, we can observe that VBG$_1$ combines two channels, however, VBG$_4$ combines four transmitting channels and one diffracting channel. Given that commercially available PTR-glass-based VBGs have a thermal expansion coefficient as low as 10^{-5}/K [18], so the thermal stress on the VBG is not a major factor to be considered. Unfortunately, VBGs are temperature dependent elements which have a wavelength shift coefficient of approximate 0.01 nm/K. In such a cascaded DSC structure, every successive VBG experiences increasing power radiation and thermal load, so causing different Bragg wavelength shift. The distance between two first minimum of VBG spectral selectivity is usually designed to only 0.4–0.6 nm, therefore it easily produces a major loss if the spectrum of the block is unable to match Bragg wavelength of VBG. Hence, the temperature control of reflecting VBGs will provide a solution to maintain the combining efficiency. In our case, four thermo-electric coolers (TECs) are mounted on the each VBG. These TECs can provide VBG temperature control ranging from 293.0 K to 340.0 K with an accuracy of about 0.1 K. A temperature sensor is laterally attached to the VBG. Through monitoring the operating temperature of the individual VBG and employing a temperature control, the temperature difference of VBGs can be controlled within ±1 K.

Fig. 6 shows the curves of the combining efficiency of the 97× nm submodule with and without temperature control. At the preliminary stage where the pump current is less than 7 A, two curves display a similar tendency. The combining efficiency is raised with the increasing pump current,
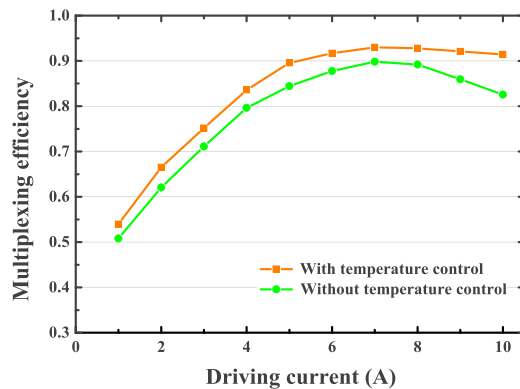
Fig. 6. The curves of the measured combining efficiency with and without temperature control.

TABLE 1

The Wavelength Channels of Four Submodules

	Channel 1	Channel 2	Channel 3	Channel 4	Channel 5
Module 1 (91× nm)	913.1	914.5	916.0	917.5	919.1
Module 2 (94× nm)	941.3	942.7	944.4	945.8	947.3
Module 3 (97× nm)	973.1	974.5	976.1	977.6	979.0
Module 4 (102× nm)	1017.2	1018.5	1020.1	1021.5	1022.8

because the spectrum of the submodule is gradually close to Bragg wavelength of VBG. At the pump current above 7 A, two curves show the difference in the combining efficiency. Without the temperature control, the combining efficiency reduces to approximate 83% because of the rising temperature of VBGs. However, when the temperature control is employed, the combining efficiency increases to 94%.

According to the process mentioned above, similar results are obtained with other three submodules operating at 91×, 94× and 102× nm. The wavelength of all channels are shown in the following Table 1.

After DSC, a pair of submodules with the same wavelength are polarization multiplexed to realize a high power module which can output the doubled power while maintaining a constant beam quality. In polarization beam combination (PBC), a half-waveplate is used to rotate the horizontal polarization state of one beamlet to vertical direction, which makes the polarization states of two beamlets orthogonal. Subsequently, the two orthogonally polarized beamlets are multiplexed together when they reach the polarization beam splitter (PBS).

3.3 Coarse Spectral Combination

In the second stage, the technology of CSC is employed to combine four different wavelength modules by dielectric mirrors which are typically designed for transmitting the long wavelength channel and reflecting the short one to obtain a high combining efficiency. The size of the dielectric mirrors is 10 mm × 10 mm, and the thickness is 3 mm. Fig. 7 is the schematic diagram of CSC, the first dielectric mirror combines two beamlets from 91× and 94× nm modules, whereas the final one combines three reflecting beamlets from 91×, 94× and 97× nm modules and one transmitting beamlet from 102× nm module.

The power radiated on the dielectric mirrors is several times higher than that on the VBGs. Despite the combining efficiency of dielectric mirrors is temperature independent, the increase of laser radiation and thermal load lead to a thermal expansion of dielectric mirrors. This not only affects the beam quality, but also causes the thermal stress which can bring a risk for the reliability
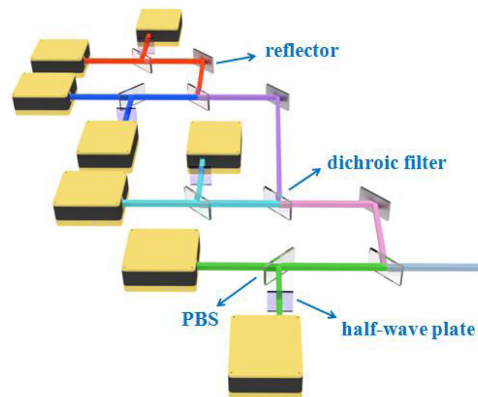
Fig. 7. Schematic diagram of CSC. The wavelengths of submodules are 915 nm (red beam), 940 nm (dark blue beam), 976 nm (light blue beam), and 1020 nm (green beam)
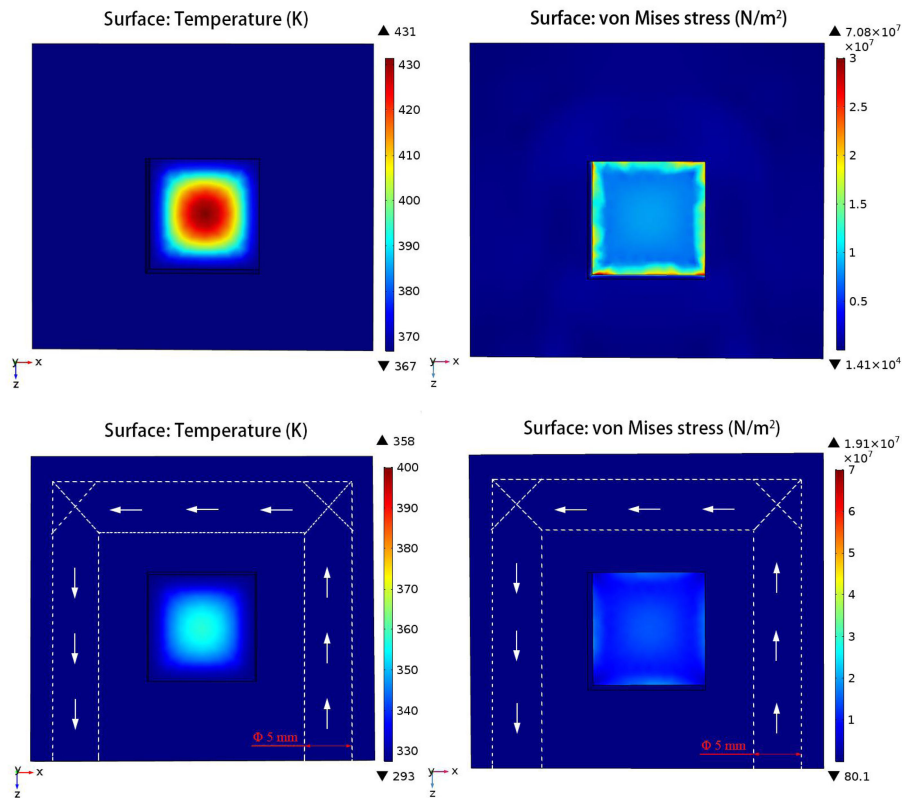

Fig. 8. Simulations of temperature (top left) and thermal stress distribution (top right) without water cooling, and temperature (bottom left) and thermal stress distribution (bottom right) with water cooling.

of dielectric mirrors. Therefore, it is important to research the thermal management of dielectric mirrors to minimize the thermal stress. In this system, the final dielectric mirror is most damaged due to sustaining the highest power of radiation, so we use a thermal analysis software COMSOL to illustrate its temperature variation and thermal stress, which are shown in Fig. 8. When the dielectric mirror is in the condition of free convection cooling, the temperature of central range of dielectric mirror is 431.0 K, corresponding to a von Mises stress of 70.8 MPa, which can lead to the
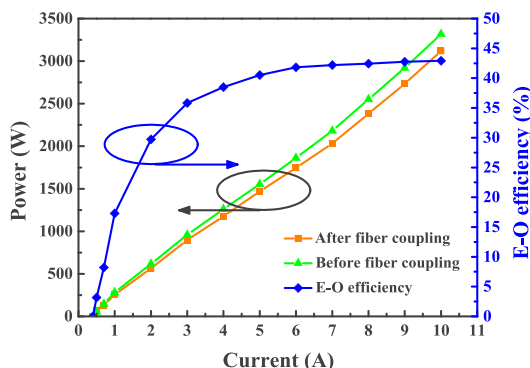
Fig. 9. Output power and E-O efficiency versus pump current. The temperature of coolant water for diode laser blocks is set to be 298 K.

deformation of the dielectric mirror. As the heat dissipation ability of TEC is limited, water cooling is instead used to control the temperature of dielectric mirrors. In our case, dielectric mirrors are surrounded by water-cooled holders in which the flowing water can efficiently remove the thermal loads of VBGs and reduce the thermal stress. The flux of cooling water is set to be 6 L/min, and the temperature is set to be 295.0 K. As a result, the maximum temperature is significantly reduced from 431.0 K to 358.0 K, and the corresponding maximum von Mises stress is reduced from 70.8 MPa to 19.1 MPa. By this way, this diode laser source can operate under a safe condition.

4. Results and Analysis

After the stage of CSC, the beam quality analyzer is used to measure the beam quality of combined beam, and BPP of 4.5 mm ·mrad is obtained at a pump current of 10 A. Afterwards, an aspherical lens is employed to couple the combined beam into a commercially available quartz block high-power (QBH) fiber with 105 μm core diameter and 0.2 NA. A CW power of 3120 W and an E-O efficiency of 42.9% are realized (Fig. 9). This corresponds to a brightness of 1031 MW/(cm^2·sr). This system shows high stability in the hours of operation, and the observed output power is fluctuant less than 3%.

However, the optical-optical (O-O) efficiency η_{o-o} is finally limited to 78%. The O-O efficiency is defined as

$$\eta_{o-o} = \frac{P_{ex}}{\sum P_{emitter,i}}, \tag{4}$$

where P_{ex} is the power output from the optical fiber, and $P_{emitter,i}$ is the free-running power of the single emitter at 10 A. The following points can account for major reasons of the power loss.

1) In the process of the optical stacking, to maximize the filling density, marginal part of beams emitted from single emitters are blocked out by reflectors, which can lead to about 3.5% power loss.

2) In DSC of 91×, 94×, 97× and 102× nm, we obtain a combining efficiency of approximate 92% at a pump current of 10 A. This value is still lower than the theoretical result (96%) calculated by Eq. (5) [19]

$$\eta_{total}(N) = \frac{1}{N}\left(\eta_T^{N-1} + \eta_D \frac{1 - \eta_T^{N-1}}{1 - \eta_T}\right). \tag{5}$$

The difference in the combining efficiency mainly due to cross-talk effects between locking spectrums and the spectral selectivity of VBGs.

3) Combining elements of PBSs and dielectric mirrors have the same combining efficiency. Usually, the combining efficiency is 96% for transmitting beamlet and 99% for reflecting beamlet, which can cause loss at each step of PBC and CSC.

4) The coupling efficiency is approximate 94% at the pump current of 10 A. The efficiency η_{FC} is defined as

$$\eta_{FC} = \frac{P_{ex}}{P_{CSC}}, \tag{6}$$

where P_{CSC} is the power after CSC. Since the long wavelength range of combined beam from $91\times$ nm to $102\times$ nm can cause the focal chromatic aberration, the focal point overfills the diameter of the optical fiber core, therefore the power loss is induced.

5. Summary and Conclusion

In this paper, we have demonstrated a structure of two-stage combination with DSC and CSC. By investigating thermal effects and the temperature control for combining elements, we address critical issues such as the spectral mismatch of VBGs and thermal stress on the dielectric mirrors. Consequently, a direct diode laser source which can produce 3120 W output power is realized at a pump current of 10 A. The optical fiber is 105 μm and 0.2 NA.

Compared to the technology of WBC, we use the commercial diode laser blocks to obtain high output power, which is a way to increase the stability and decrease development costs. Integrating a structure of distributed Bragg reflector or distributed feedback in diode laser chips to narrow the spectrum is also a promising approach for DSC [20], but this technology requires a specific semiconductor manufacturing process. We have shown that our proposed method has no such high demand for diode laser chips.

References

[1] H. Zhu *et al.*, "Development and thermal management of 10 kW CW, direct diode laser source," *Opt. Laser Technol.*, vol. 76, pp. 101–105, Jan. 2016.

[2] G. C. Rodrigues, J. Pencinovsky, M. Cuypers, and J. R. Duflou, "Theoretical and experimental aspects of laser cutting with a direct diode laser," *Opt. Lasers Eng.*, vol. 61, pp. 31–38, Oct. 2014.

[3] J. J. Lim *et al.*, "Design and simulation of nest-generation high-power, high-brightness laser diodes," *IEEE J. Sel. Topics Quantum Electron.*, vol. 15, no. 3, pp. 993–1008, May 2009.

[4] S. M. Redmond *et al.*, "Active coherent beam combining of diode lasers," *Opt. Lett.*, vol. 36, no. 6, pp. 999–1001, Mar. 2011.

[5] G. Schimmel *et al.*, "Rear-side resonator architecture for the passive coherent combining of high-brightness laser diodes," *Opt. Lett.*, vol. 41, no. 5, pp. 950–953, Feb. 2016.

[6] R. K. Huang *et al.*, "TeraDiode's high brightness semiconductor lasers," *Proc. SPIE*, vol. 9730, Mar. 2016, Art. no. 97300C.

[7] S. Hengesbach, S. Klein, C. Holly, U. Witte, M. Traub, and D. hoffmann, "Simultaneous Frequency stabilization and high-power dense wavelength division multiplexing (HP-DWDM) using an external cavity based on Volume Bragg Grating (VBGs)," *Proc. SPIE*, vol. 9733, Mar. 2016, Art. no. 97330K.

[8] F. Ferrario *et al.*, "Building block diode laser concept for high brightness laser output in the kW range and its applications," *Proc. SPIE*, vol. 9733, Mar. 2016, Art. no. 97330G.

[9] B. Leonhauster, H. Kissel, A. Unger, B. Kohler, and J. Biesenbach, "Feedback-induced catastrophic optical mirror damage (COMD) on 976 nm broad area single emitters with different AR reflectivity," *Proc. SPIE*, vol. 8965, Feb. 2014, Art. no. 896506.

[10] R. Lang and K. Kobayashi, "External optical feedback effects on semiconductor injection laser properties," *IEEE J. Quantum Electron.*, vol. 16, no. 3, pp. 347–355, Apr. 1980.

[11] Y. Li *et al.*, "Wavelength locking of high-power diode laser bars by Volume Bragg Gratings," *IEEE Photonics Society Summer Topical Meeting Series*, Jul. 2012.

[12] C. Holly, S. Hengesbach, M. Traub, and D. Hoffmann, "Simulation of spectral stabilization of high-power broad-area edge emitting semiconductor lasers," *Opt. Exp.*, vol. 21, no. 13, pp. 15553–15567, Jul. 2013.

[13] B. Leonhauser, H. Kissel, J. W. Tomm, M. Hempel, A. Unger, and J. Biesenbach, "High-power diode lasers under external optical feedback," *Proc. SPIE*, vol. 9348, Apr. 2015, Art. no. 93480M.

[14] U. Witte *et al.*, "kW-class direat diode laser for sheet metal cutting based on DWDM of pump modules by use of ultra-steep dielectric filters," *Opt. Exp.*, vol. 24, no. 20, pp. 22917–22929, Oct. 2016.

[15] P. Leisher *et al.*, "Reliability of high power diode laser systems based on single emitters," *Proc. SPIE*, vol. 7918, Feb. 2011, Art. no. 791802.

[16] K. Price, S. Karlsen, P. Leisher, and R. Martinsen, "High brightness fiber coupled pump laser development," *Proc. SPIE*, vol. 7583, Feb. 2010, Art. no. 758308.

[17] R. Liu *et al.*, "High brightness 9× nm fiber coupled diode lasers," *Proc. SPIE*, vol. 9348, Mar. 2015, Art. no. 93480V.

[18] D. R. Drachenberg, O. Andrusyak, G. Venus, V. Smirnov, and L. B. Glebov, "Thermal tuning of volume Bragg gratings for spectral beam combining of high-power fiber lasers," *Appl. Opt.*, vol. 53, no. 6, pp. 1242–1246, Feb. 2014.

[19] A. Sevian, O. Andrusyak, I. Ciapurin, V. Smirnov, G. Venus, and L. Glebov, "Efficient power scaling of laser radiation by spectral beam combining," *Opt. Lett.*, vol. 33, no. 4, pp. 384–386, Feb. 2008.

[20] U. Witte *et al.*, "Compact 35 μm fiber coupled diode laser module based on dense wavelength division multiplexing of NBA mini-bars," *Proc. SPIE*, vol. 9733, Mar. 2016, Art. no. 97330H.